Energy 82 (2015) 193–205

Contents lists available at ScienceDirect

Energy

journal homepage: www.elsevier.com/locate/energy

# THM (Thermo-hydro-mechanical) coupled mathematical model of fractured media and numerical simulation of a 3D enhanced geothermal system at 573 K and buried depth 6000–7000 M

Yangsheng Zhao*, Zijun Feng, Zengchao Feng, Dong Yang, Weiguo Liang

*Mining College of Taiyuan University of Technology, Taiyuan 030024, China*

ARTICLE INFO

*Article history:*
Received 23 May 2014
Received in revised form
24 November 2014
Accepted 11 January 2015
Available online 7 February 2015

*Keywords:*
Hot dry rock
THM (thermo-hydro-mechanical) coupled simulation
Fracture aperture
Temperature
Water pressure
Output and lifespan

ABSTRACT

Hot dry rock geothermal energy is almost inexhaustible green energy. However, it makes slow progress in practice due to slow theory development. In this study, a three dimension thermo-hydro-mechanical coupled model of fractured media was established to simulate the extraction of HDR (Hot dry rock) geothermal energy based on the geological characteristics (geothermal gradient of 50 K/km, buried depth of 6250–6750 m) of Tengchong geothermal field in China. The simulation results show the variation in both field of temperature, stress, seepage and fracture aperture during heat extraction. The temperature in fracture face increased exponentially from injection well towards production well while extracting heat. The initial rock mass temperature of 573 K decreases to 423 K after 9-year running. The initial water pressure gradient in the fracture reached 0.17 MPa/m near the injection well and then decreased to 0.052 MPa/m after 1 year. The fracture aperture was triple of the initial value and the permeability coefficient increased by nine times over the 9-year operation period. That seepage resistance of artificial storage reservoir gradually decreased could improve extracting geothermal energy more efficiently. The amount of extracted heat declined exponentially with running time. The total extracted geothermal energy over 9 years was 5977 MWa and rock mass temperature decreased to 423 K.



## 1. Introduction

HDR (Hot dry rock) geothermal energy is an inexhaustible energy resource. Large-scale investigations [1–3,7,9,12–14], were conducted around the world following the successful testing of the United States Fenton Hill geothermal site in 1984. In these studies a new type of enhanced geothermal system was proposed in which an artificial storage layer is created by multiple vertical cracks produced by horizontal drilling. The studies investigated the heat exchange, heat transfer, fluid migration, rock mass deformation, and the coupling effect surrounding an EGS (enhanced geothermal system) underground artificial heat exchange system. Kohl et al. [4] modeled coupled THM (thermo-hydro-mechanical) processes in a single fracture using linear thermo-poroelastic effects. Taron and Elsworth [15] studied THMC (thermo-hydro-mechano-chemo) coupling effects in dual porosity media where porosity and permeability change as a result of changes in stress and chemical precipitation and dissolution. Pandey et al. [10] investigated the evolution of the fracture aperture under the effects of THC (thermo-hydro-chemical) coupling. Ghassemi and Zhou [11] coupled fracture flow and heat transport to thermo-poroelastic deformation in a discretely fractured reservoir and examined the changes in temperature, pressure, and aperture with time. Fox et al. [8] studied multi-fracture systems, and derived the temperature mass flow law for geothermal energy extracted at fracture spacing of 200 m, 100 m, and 50 m. Zeng et al. [5,6] investigated HDR in the Desert Peak geothermal field in American through a single vertical fracture and horizontal fracture. The underground heat exchange system included complex convection heat transfer and heat exchange in fractured media, water migration, and rock mass deformation. They also considered chemical dissolution and diffusion caused by changes in the HDR with depth and scale.

It is more special for numerical simulation of hot dry rock geothermal energy extraction to consider coupling effect of hot fluid transmission-fractured rock mass deformation-heat transfer in artificial hydrofracturing. In particular less studies is conducted on the variations of stress field, fracture opening, permeability during extracting geothermal energy from hot dry rock. However,

* Corresponding author. Tel.: +86 0351 6014865.
*E-mail address:* y-s-zhao@263.net (Y. Zhao).

http://dx.doi.org/10.1016/j.energy.2015.01.030
0360-5442/

**Nomenclature**

| | |
|---|---|
| $\lambda$ | one of the lame constant [M L$^{-1}$ T$^{-2}$] |
| $\mu$ | one of the lame constant [M L$^{-1}$ T$^{-2}$] |
| $U_i$ | solid displacement component [L] |
| $F_i$ | applied to rock mass body force component [M L$^{-2}$ T$^{-2}$] |
| $\beta_s$ | $\beta_s = \alpha E/(1-2\nu)$ [M L$^{-1}$ T$^{-2}$] |
| $\alpha$ | linear thermal expansion coefficient of rock [K$^{-1}$] |
| $E$ | elastic modulus [M L$^{-1}$ T$^{-2}$] |
| $\nu$ | poisson's ratio |
| $T$ | temperature [K] |
| $t$ | time [T] |
| $T_r$ | temperature of rock matrix [K] |
| $K_n$ | crack normal stiffness [M L$^{-1}$ T$^{-2}$] |
| $K_s$ | crack tangential stiffness [M L$^{-1}$ T$^{-2}$] |
| $\sigma'_n$ | effective normal stress component to fracture [M L$^{-1}$ T$^{-2}$] |
| $\sigma'_s$ | effective tangential stress component to fracture [M L$^{-1}$ T$^{-2}$] |
| $\varepsilon_n$ | normal strain component to crack |
| $\varepsilon_s$ | tangential strain component to crack |
| $\sigma_n$ | total normal stress component to crack [M L$^{-1}$ T$^{-2}$] |
| $P$ | water pressure in pore or crack [M L$^{-1}$ T$^{-2}$] |
| $\beta_A$ | ratio of the connected area to total area of crack |
| $K$ | Kelvin temperature unit |
| $cpr$ | specific heat of the rock matrix [L$^2$ T$^{-2}$ K$^{-1}$] |
| $cpw$ | specific heat of the water [L$^2$ T$^{-2}$ K$^{-1}$] |
| $\rho_r$ | density of rock matrix [M L$^{-3}$] |
| $\lambda_r$ | thermal conductivity of rock-matrix [M L T$^{-3}$ K$^{-1}$] |
| $W$ | source sink term of heat [M L$^{-1}$ T$^{-3}$] |
| $\rho_w$ | density of water [M L$^{-3}$] |
| $T_w$ | water temperature [K] |
| $\lambda_w$ | thermal conductivity of water [M L T$^{-3}$ K$^{-1}$] |
| kfi | water permeability coefficient in I crack [L T$^{-1}$] |
| Trb | fracture surface temperature [K] |
| $b$ | crack aperture [L] |
| $q_i$ | water specific flux [L T$^{-1}$] |
| $\Phi$ | crack porosity |
| $\beta_2$ | water compressibility |
| $e$ | rock matrix volume deformation |
| $s$ | crack tangential coordinates [L] |
| $\sigma'_{ij}$ | effective stress tensor [F L$^{-2}$] |
| $\varepsilon_{ij}$ | strain tensor |
| $\varepsilon_{kk}$ | volume strain |
| $\delta_{ij}$ | kronecker symbol |
| $\delta_w$ | function of p and T, not exceed 6% of $1/\rho_w$ |

these changes will have significant influence on economic profits and sustainability of extracting hot dry rock geothermal energy. Further theoretical research and numerical simulation of HDR geothermal energy extraction is still needed. Very few investigations of topics such as EGS construction at high temperature and depth, analyses of rock mass deformation and fracture, and heat transfer and pressure variation have been carried out under the relatively strict THM coupling effect.

In the paper, a theoretical model of fractured rock mass deformation, seepage, and heat transfer was established with a combination of fine and coarse grids and numerically simulated fracture faces of injection and production wells in the HDR EGS. The modeling included variations in temperature, stress, and fluid pressure of rock mass at depth of 6000–7000 m and temperature of 573 K. This model investigated the evolution of aperture, water pressure, and temperature in fracture, and the evolution of the heat extraction capacity in the constant pressure mining system with time. In addition, the heat recovery of the geothermal extraction system after the mining ended was analyzed.

## 2. Mathematical model of fractured media THM coupling

### 2.1. Physical considerations

In the geothermal extraction system, the rock mass as a direct carrier of fluid migration and heat transfer can be simplified as a fracture media model consisting of a matrix rock block and a fracture. When establishing the mathematical model of the fractured media THM coupling, we assumed the following:

(1) The rock mass structure is composed of fractures and a matrix rock block of dual media containing pores and cracks.
(2) The matrix rock block of the rock mass can be simplified as continuous media with homogeneous isotropic elastomers; the rock mass fracture can be simplified as fracture media.
(3) Compared with the fissures, the water storage capacity and water permeability of the matrix rock block are very weak; thus, they can be neglected in the mathematical model.
(4) The fracture seepage law complies with Darcy's Law:

$$q_i = -k_{fi}\frac{\partial p}{\partial s_i} \quad i = (1,2) \tag{1}$$

where $k_{fi} = (b^2/12)$ is the fracture permeability coefficient and $b$ is the fracture aperture, $p$ is pressure of fracture, $s_i$ is a coordinates along with surface fracture.

(5) The fracture deformation agrees with the joint unit model.
(6) The water does not vaporize because it is under high pressure; we assume that the rock mass is saturated with single-phase water.
(7) The effective stress law of rock mass fracture is $\sigma' = \sigma - \beta_A p$, where $\beta_A$ is the ratio of the connectivity area to the total area in the rock mass fracture.
(8) The matrix rock blocks comply with the thermo-elastic constitutive law as follows:

$$\sigma'_{ij} = \lambda\delta_{ij}\varepsilon_{kk} + \frac{E}{1+\nu}\varepsilon_{ij} - \frac{E}{1-2\nu}\alpha\Delta T\delta_{ij} \tag{2}$$

where $\alpha$ is the thermal expansion coefficient of the rock mass [1/K], $\Delta T$ is the temperature increment of the rock mass, $E$ is the elastic modulus, $\nu$ is Poisson's ratio, $\lambda$ is the Lamé constant, and $\delta_{ij}$ is the Kronecker symbol.

(9) The density of the water is no longer a constant but a function of pressure and temperature, $\rho_w = \rho_w(p, T_w)$ and is expressed as follows:

$$\frac{1}{\rho_w} = 3.086 - 0.899017(4014.15 - T)^{0.147166} - 0.39(658.15 - T)^{-1.6}(p - 225.5) + \delta_w \quad (3)$$

where $\rho_w$ is water density [g/cm$^3$], $T$ is the water temperature [K], $p$ is water pressure [absolute Atm], and $\delta_w$ is a function of $p$ and$T$; in general, the value of $\delta_w$ does not exceed 6% of $1/\rho_w$.

(10) Rock mass heat can be transferred in three ways: conduction, convection, and radiation. In this study we assumed that the radiation components may be neglected.
(11) The flow of water is by forced convection; the water flow rate does not depend on density or viscosity.

### 2.2. Mathematical model

Based on the above assumptions, the mathematical model of fractured media THM coupling can be expressed as follows:

The deformation equation of the matrix rock block:

$$(\lambda + \mu)U_{j,ji} + \mu U_{i,jj} + F_i - \beta_s T_{,i} = 0 \quad (4)$$

The deformation equations of the rock mass fracture:

$$\begin{aligned} \sigma_n' &= k_n \varepsilon_n \\ \sigma_s' &= k_s \varepsilon_s \\ \sigma_n' &= \sigma_n - \beta_A p \end{aligned} \quad (5)$$

The temperature field equation of the matrix rock block:

$$\rho_r c_{pr} \frac{\partial T_r}{\partial t} = \lambda_r T_{r,ii} + W \quad (6)$$

The water temperature field equation of the rock mass fracture:

$$c_{pw} \frac{\partial(\rho_w T_w)}{\partial t} = \lambda_w \nabla^2 T_w - c_{pw} \cdot \left(\rho_w \cdot k_{fi} \cdot p_{,i} \cdot T_w\right)_{,i} + \frac{2\lambda_r}{b}(T_{rb} - T_w) \quad (7)$$

The water seepage control equation of the rock mass fracture:

$$div(\rho_w q_i) + \varphi \cdot \beta_2 \cdot \rho_w \frac{\partial p}{\partial t} + \rho_w \cdot \frac{\partial e}{\partial t} = 0 \quad (8)$$

The seepage equation of the rock mass fracture is:

$$q_i = -k_{f_i} \frac{\partial p}{\partial s_i} \quad (9)$$

The mathematical model of the fractured media THM coupling is composed of equations (4) to (9) and the initial and boundary conditions.

This model has the following characteristics:

(1) The solid deformation equation analyzes the effects of heat stress. In Eq. (4), the temperature factor $\beta T_{,i}$ is added to the common elastic mechanic equation. Note that the model neglects the effects of seepage because of the very low permeability of the matrix rock block.
(2) The water density is no longer a constant but a function of the water pressure and temperature, $\rho_w = \rho_w(p, T_w)$.
(3) The water temperature field equation of the rock mass fracture describes the heat transfer process with simultaneous conduction and convection, which is generally more accurate than discussing simple conduction or convection.
(4) The water heat transfer equation of the fracture includes the pore pressure, while the fracture seepage and deformation equation contains the pressure parameter. Consequently, a THM multi-field coupled mathematical model is established that can represent the interactions of the water seepage, heat transfer, and deformation of the fracture and matrix rock block.
(5) Compared to the mathematical model in the literature such as Ghassemi's [11] model, the presented model contains the deformation of not only rock mass matrix but also fracture which is calculated by Goodman Joint Element, and heat conduction and convection with time in fracture.

## 3. Model simplification and numerical analyses of geothermal energy extraction from hot dry rock

In this study, the HDR geothermal energy extraction in Tengchong, Yunnan province of China is taken as a case study of the effect of THM-coupled interaction on a deep HDR geothermal extraction system.

### 3.1. Experimental zone overview and model simplification

The Yunnan Tengchong region is a typical HDR zone with extremely rich geothermal resources. Our model is based on the Tengchong HDR geothermal field. The model was simplified to a $5.0 \times 5.0 \times 5.0$ km$^3$ cube model at a depth of 4 km as shown in Fig. 1. An ideal numerical model of a horizontal well and vertical fracture was used to simplify the calculations (Figs. 1 and 2). In order to study the physical variation (such as temperature, water pressure, fracture opening, and etc.) in rock induced by extracting geothermal energy from hot dry rock, it is significant to understand the changes of physical characteristic not only among fractures but also between rock and fracture. Two fractures are introduced in the model to not only achieve the two goals but also simplify the physical model and reduce the compute workload. The model was set up as two parallel vertical fracture planes along the vertical direction of the minimum principal stress (x direction) 500 m apart; the coordinate locations were $x_1 = 2250$ m, $x_2 = 2750$ m. The injection and production wells lie perpendicular to the fracture

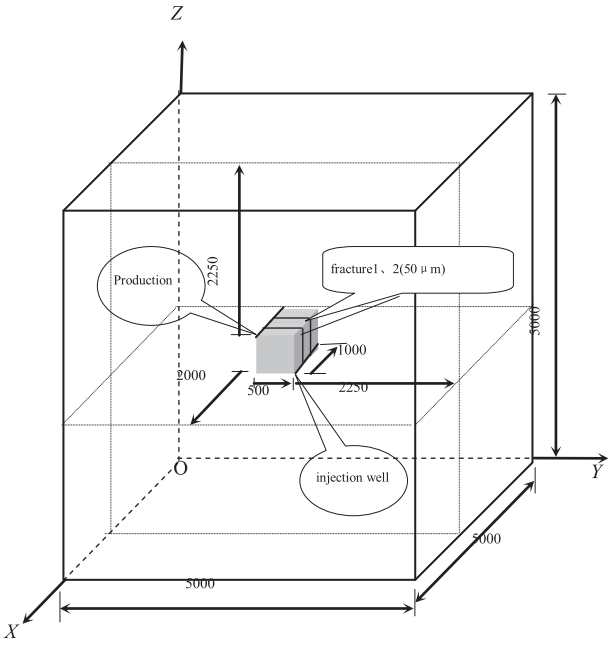


**Fig. 1.** Coordinate and dimensions of calculated model.

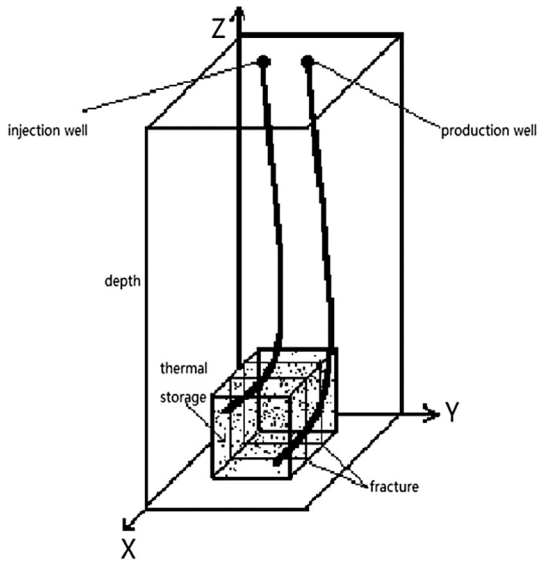


**Fig. 2.** Drilling schematic diagram.

plane (Fig. 1). The injection well is in the deeper rock layer, at coordinates (2000–3000 m, 2750 m, 2250 m); the coordinates of the production well are (2000–3000 m, 2250 m, 2750 m).

### 3.2. Boundary and initial conditions

(1) Solid deformation boundary conditions: the stress, $P_z$, at the upper part of the model exerted by the gravity of the upper rock layers was determined by the rock layer thickness as 100 MPa. To represent the effects of the tectonic stress field caused by the wall rock stress around the model, the sideways pressure coefficients were selected as 0.8 and 1.2, respectively. And the corresponding horizontal stresses of $P_x$ and $P_y$ are 80 MPa and 120 MPa. The displacement boundary conditions of the other three directions were set as zero (Fig. 3).

(2) Seepage field boundary conditions: to ensure a circulating water system in the geothermal extraction system, using a given pressure boundary condition, the given pressure of the injection well was 27.3 MPa and that of the production well was 9.8 MPa. For the other external conditions an impermeable boundary was selected because of the very low permeability of granite, $q = 0$.

(3) Temperature field boundary conditions: the heat supply was continuous because of the existing large-scale geothermal reservoir around the model. Therefore, the boundary condition for the heat flow was set up as follows: $Q = \rho_r \cdot \lambda_r \cdot \nabla T_r$, the temperature of the injected water was 303 K, and the geothermal gradient was 50 K/km.

The boundary and initial conditions are listed Table 1. The granite physical parameters used in the numerical model are shown in Table 2.

### 3.3. Solution method of the coupling model

The solid deformation, fluid seepage, and temperature field equations were regarded as independent subsystems for the solid, fluid, and thermal multi-coupling mathematical model. To obtain the numerical solution of the coupling iteration, the scatter control equation was used with the finite element discrete method

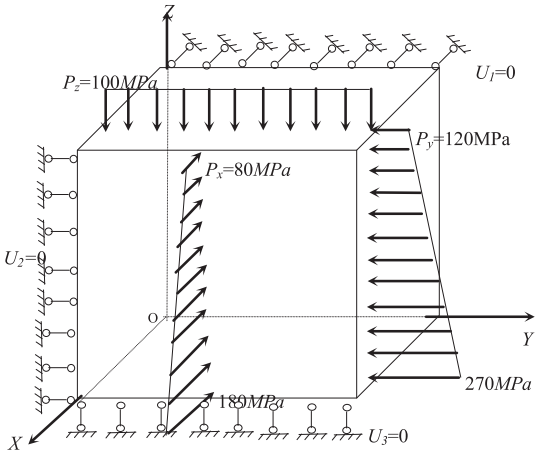


**Fig. 3.** Simplified boundary conditions of calculation model $U_1$, $U_2$, $U_3$ represent the displacement variables in x, y, z direction, respectively.

**Table 1**
The boundary and initial conditions of the coarse grid computing model.

| Items | Boundary | Boundary and initial conditions |
|---|---|---|
| Solid deformation $0 \le t < \infty$ | Z = 5000 m roof surface | Pz = 100 MPa s kind boundary |
| | Z = 0 bottom surface | Uz = 0 first kind boundary |
| | Y = 0 left surface | Uy = 0 first kind boundary |
| | Y = 5000 m right surface | Py = 120 + (5000 − Z)(270 − 120)/5000 MPa |
| | X = 5000 m before surface | Px = 80 + (5000 − Z)(180−80)/5000 MPa |
| | X = 0 behind surface | Ux = 0 |
| Seepage | Injection well (ground surface) | $P(t)_{injection}$ = 27.3 MPa, $0 \le t < \infty$ |
| | Production well (ground surface) | $P(t)_{production}$ = 9.8 MPa, $0 \le t < \infty$ |
| | Six surfaces area | q(t) = 0 is not seepage boundary, $0 \le t < \infty$ |
| | All of points (exception of wells) | P(x,y,z,0) = 50.0 MPa, t = 0 |
| Temperature | All of points | $T(x,y,z,0) = T_0 + 50$ K*z/1000, t = 0 |
| | Injection well | $T(t)_{injection}$ = 303 K, $0 \le t < \infty$ |
| | Six surfaces area | $Q = \rho_r \lambda_r \nabla T_{ri}$, $0 < t < \infty$; Q = 0, t = 0 |

(Galerkin) in the geometry domain, and then the discrete equation was obtained using the difference method in the time domain. For the finite element solution, numerical simulation of a 3-D system of HDR geothermal extraction was implemented using a method that combines fine and coarse grids in the calculation to reduce the influence of the boundary effects. While a fine grid division increases the calculation accuracy, it also increases the calculating intensity and workload. In this model, the regional center and drilling vicinity were the main research area; therefore, a 5-km zone covering the whole geothermal system was first calculated

**Table 2**
Granite physical and mechanical features parameter.

| Parameter | Unit | Matrix block | Fracture (water) |
|---|---|---|---|
| Storage coefficient | | | $7.0 \times 10^{-3}$ |
| Density | Kg $m^{-3}$ | $2.7 \times 10^3$ | $1.07 \times 10^3$ |
| Young's modulus | $MP_a$ | $4.84 \times 10^4$ | $2.84 \times 10^4$ |
| Poisson's ratio | | 0.15 | 0.25 |
| Heat transfer coefficient | W $m^{-1}$ $K^{-1}$ | 0.68 | 2.58 |
| The coefficient of heat capacity. | J $kg^{-1}$ $K^{-1}$ | $1.08 \times 10^3$ | $4.05 \times 10^3$ |
| Thermal expansion coefficient | $K^{-1}$ | $1.0 \times 10^{-5}$ | |
| Permeability | m $s^{-1}$ | $1.15 \times 10^{-9}$ | 0.111 |

using a rough calculation model (Fig. 4), then 1000 × 500 × 500 $m^3$ areas around the drilling and fracture zones of the geothermal system were calculated using a detailed calculation model (Fig. 5).

Thus, the values obtained by the rough calculation method were used as boundary conditions to reduce the influence of the boundary effects on the system. At the same time, to reduce the workload and calculating intensity, the drilling zone was arranged directly on the node and the grid division method was used as a partial increasing grid density scheme as shown in Figs. 4 and 5.

FEM (**F**inite element method) is used to solve the mathematical model for a practice case in the paper. Hexahedral eight-node isoparametric element is adopted for discrete of rock matrix while eight-node Goodman joint element for fracture area. Both the coarse and fine grids were employed to scatter compute area. In Fig. 4, coarse grid of 50 m × 50 m × 50 m generally scatters the area far away from wellbore and fractures while fine grids of 10 m × 10 m × 50 m and 10 m × 10 m × 10 m are made within 1000 m of drilling and fracture area. Joint unit is scattered by the grids of 50 m × 50 m × 0.05 mm, 10 m × 10 m × 0.05 mm and 10 m × 50 m × 0.05 mm. For the most significant research area shown in Fig. 5, the grids of 5 m × 5 m × 10 m and 5 m × 5 m × 0.05 mm are generally adopted to scatter rock mass matrix and fracture area, respectively. The grid of 5 m × 5 m × 5 m is further used to increase grid density in the rock mass matrix in the vicinity of both sides of fracture. The hexahedron isoparametric and Goodman joint elements are applied to each rock mass matrix grid and fracture grid, respectively. This grid division method not only greatly improve calculation precision but also eliminate the deviation induced by inappropriately selected boundary conditions which have some significant effect on the long term extracting area and heat recovery after extraction. Difference method is employed to calculate time. The initial time step is 10 s and acceleration factor is 1.05. It is validated by repeated calculation to be stable and reliable for compute results.

## 4. Results and discussion

### 4.1. Variations in the IP cross-section rock mass temperature

Heat transport was implemented through a plane connecting the fractures and the two wells in the HDR geothermal extraction system. The cross-section IP is the plane connecting the injection well and production well (Fig. 6). The model uses points #1–#11 along the IPF line (Fig. 6) on the fracture face as sampling points. Fig. 7a–f shows the temperature distribution along the IP cross-section. The low-temperature water from the injection well flows into the production well through the fractures (Fig. 7); the water temperature rises through convection and conduction from the high-temperature rock mass, resulting in superheated water in the production well. The rock mass temperature decreased rapidly around the injection well because of the large temperature difference between the injected low-temperature water and the high-temperature rock mass. Therefore, during the initial operation period, a relatively low-temperature area was formed. As the mining operation continued, the system temperature gradually decreased, and the low-temperature area gradually expanded. The rock mass temperature was 388 K around the injection well after the system had been running for 37 days; it decreased to 372 K on the 86th day and then remained almost constant for a longer time. The rock mass temperature decreased to 369 K and after about 1 year was down to 364 K and continued to gradually decrease after about 2 years (694 days). The rock mass temperature decreased to 330 K after about 9 years. The injection well area temperature decreased from 573 K to 405 K after running for 9 years.

To illustrate the temperature distribution and geothermal transfer between the production well and the injection well, we plotted the temperature curves along the IP cross-section at

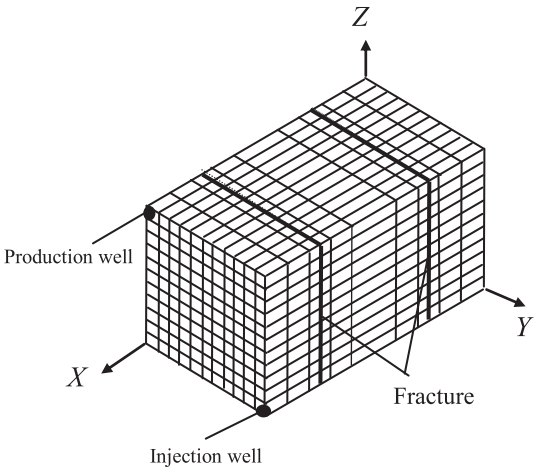


**Fig. 5.** Fine mesh dissection model (1000 m × 500 m × 500 m).

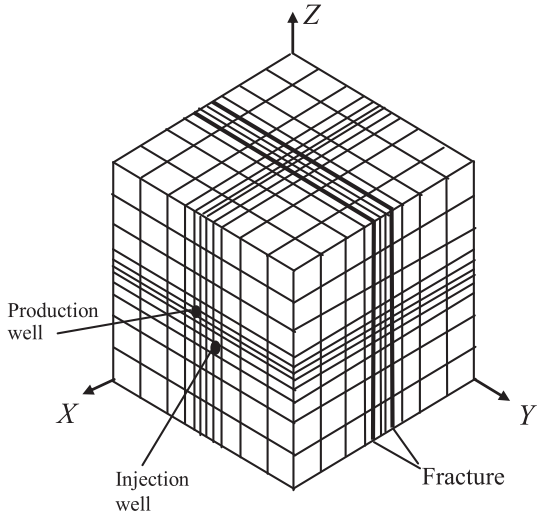


**Fig. 4.** Coarse grid model subdivision (5000 m × 5000 m × 5000 m).

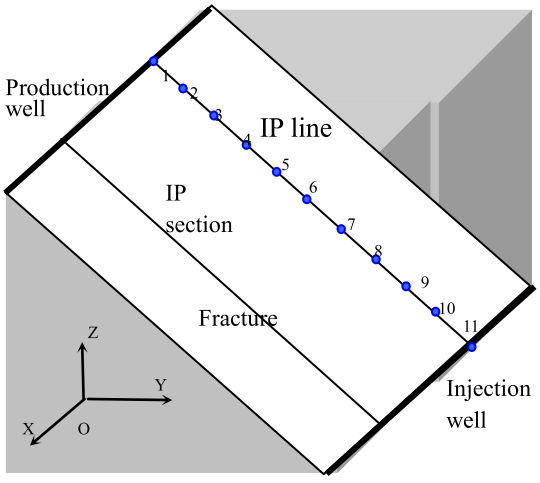


**Fig. 6.** The section between injection well and production well.

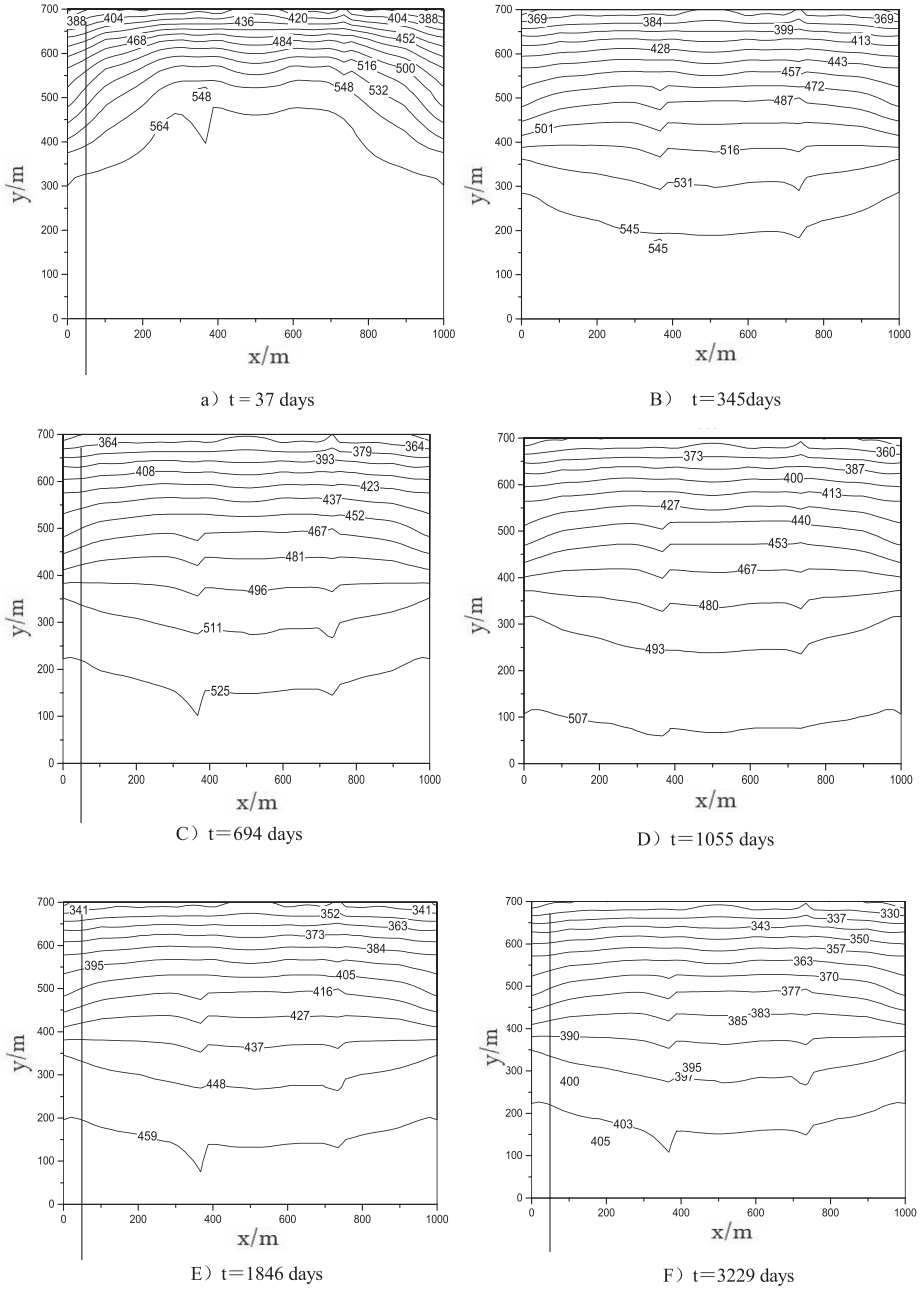


**Fig. 7.** Temperature (unit: K) distribution on the section between injection well (y = 700) and production well (y = 0).

different times during the extraction operation (Fig. 8). The temperature of the injected water increased as the water flowed into the production well; however, the heating process and heat migration pattern changed with time. In the initial period of operation, the production well produced high-temperature superheated water of 573 K and the temperature was maintained at 570 K for about 170 days. The temperature of the superheated water injected into the production well gradually decreased as the mining operation continued. After running for 9 years, the temperature of the production well was only 330 K. Thus, although the temperature of the water injected into the production well through the rock mass fractures remained the same, the heating rate gradually decreased with time. The temperature slope gradient at day 171 was much greater than that at day 3229. The distance between the injection well and the production well was divided into three sections as follows: I (0–200 m); II (200–500 m); III (500–700 m). In section I the temperature rapidly increased, in section II the heating rate slowly decreased, and in section III the temperature rise was very small, showing an almost stable temperature.

### 4.2. Temperature changes in the IPF line with operation time

The temperature change of the IPF line was analyzed from point #1 to point #11 as shown in Fig. 9. For convenience, the model only calculated the geothermal energy extraction over a period of 9 years. Overall, the temperature tended to decrease with time as shown in Fig. 9. Point #11 was the injection position, where the temperature

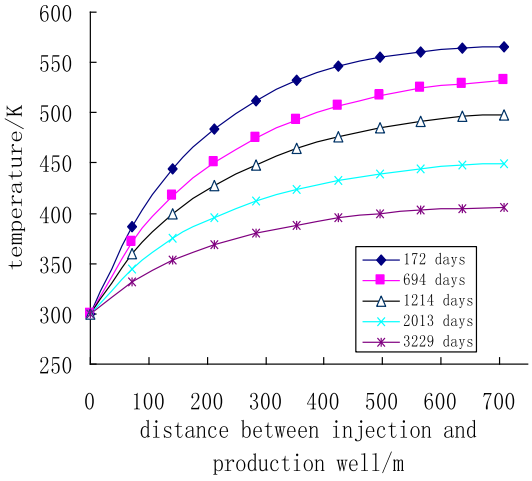


**Fig. 8.** Water temperature change between the injection well and production well over time.

was maintained at 300 K. The temperature at points #6–#11 decreased logarithmically; the initial rate of temperature decline gradually slowed and the temperature differences between the points were large. The temperatures at the points close to the production well, points #1–#5, decreased linearly, and temperature differences between the points were small. At the same time, the tendency of the temperature change varied along the cross-section. The temperature at point #10 decreased rapidly for about one season, reaching 400 K, and continued to decrease. However, at points #1, #2, and #3 the temperature remained at 570 K. Thus, the temperature change was divided according to the time period; the rate of temperature decrease around the injection well was high for about 3 years, and was much greater than that around the production well. The temperature decline rates surrounding the injection well and the production well became more gradual with time. In addition, the rate of temperature change around the production well was relatively high and gradually tended to consistency with injection well.

### 4.3. Variation of fracture face temperature with time

The temperature distribution along fracture face 1 (Fig. 2) is shown in Fig. 10a–f. The low-temperature zone with the injection well as its center gradually expanded with time, and formed a temperature field in which the temperature gradually increased from the injection well wall rock towards the production well. The temperature gradient was highest near the injection well and gradually decreased towards the production well.

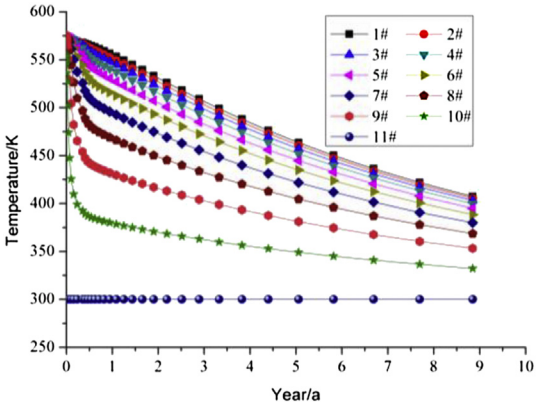


**Fig. 9.** Temperature change of point #1–#11 with extraction time.

### 4.4. Variation of fracture water pressure in the process of geothermal extraction

Fig. 11a–d display the water pressure distribution in the cross-section shown in Fig. 6. To obtain a smooth-running system, the pressure at the ground wellhead was fixed, as described in the boundary conditions above, namely the pressure of the injection well was 27.3 MPa and the pressure of the production well was 9.8 MPa. The injected low-temperature water flows to the production well along the fractures under the effects of high pressure. In the initial running stage, water flowed mostly through the fractures, and the initial water pressure of the matrix rock block was almost constant at 50 MPa. The water pressure of the matrix rock block gradually increased as the seepage accumulated; it was approximately in accordance with the water pressure of the fractures after about 180 days of operation. The area of decreasing pressure gradually broadened towards the production well. The water pressure of the whole system remained stable for about 1 year, the water circulating through the fractures with a fixed pressure gradient, keeping the HDR geothermal extraction system running effectively.

The water pressure rapidly increased in the first 6 months of operation (Fig. 12). The pressure gradient reached 0.17 MPa/m after 60 days at injection well points #9–#11 over a range of 140 m, and then the gradient gradually decreased. The geothermal extraction system remained mostly stable after 1 year of operation. The pressure gradient was larger in the areas close to the injection well and the production well as shown in Fig. 13, while the pressure gradient of the intermediate area was smaller: the pressure gradient at points #9–#11 was 0.052 MPa/m, and at points #1–#4 it was 0.04 MPa/m, but at points #4–#9 the pressure gradient was only 0.018 MPa/m. This result agrees with the results of Ghassemi [11]; however, Zeng [5,6] showed that the pressure of the fracture pores increases with time; we assume that his result may apply only in special cases.

### 4.5. Variation of the fracture face normal stress with time

The normal stress distribution for fracture face 1 (Fig. 2) is shown in Fig. 14a–f. The temperature of the wall rock decreased because of the injected low-temperature water, causing shrinkage and deformation of the wall rock, and a decrease in the stress of the rock mass, forming a further stress decline area. For a detailed illustration we selected units #1–#5 to represent the fracture face (Fig. 15). The temperature of units #2 and #3 rapidly decreased after about 1 month of operation as shown in Fig. 16; their temperature change rates were much greater than those of units #1, #4, and #5. This caused the stress around the injection well to quickly decrease (Fig. 17) and form a low-stress area. The stress at unit #1 changed exponentially with time while the stress at unit #3 changed logarithmically. Moreover, the change rates of units #1, #4, and #5 were relatively large. The area around the injection well was a low-stress area where the normal stress of the fracture face decreased by about 50% while maintaining a high tensile stress. However, Ghassemi [11] reported that tensile stress was found around the injection well and production well. Compared with Ghassemi, the results of this paper are more realistic, and the result of Ghassemi may be related to the simplified model used.

### 4.6. Variation of the fracture aperture with time

Taking 50 μm as the initial fracture aperture, the variation of the fracture aperture with time was investigated using numerical simulation, selecting representative units #1–#5 (Fig. 15) for illustration. In general, the width of the fracture face increased

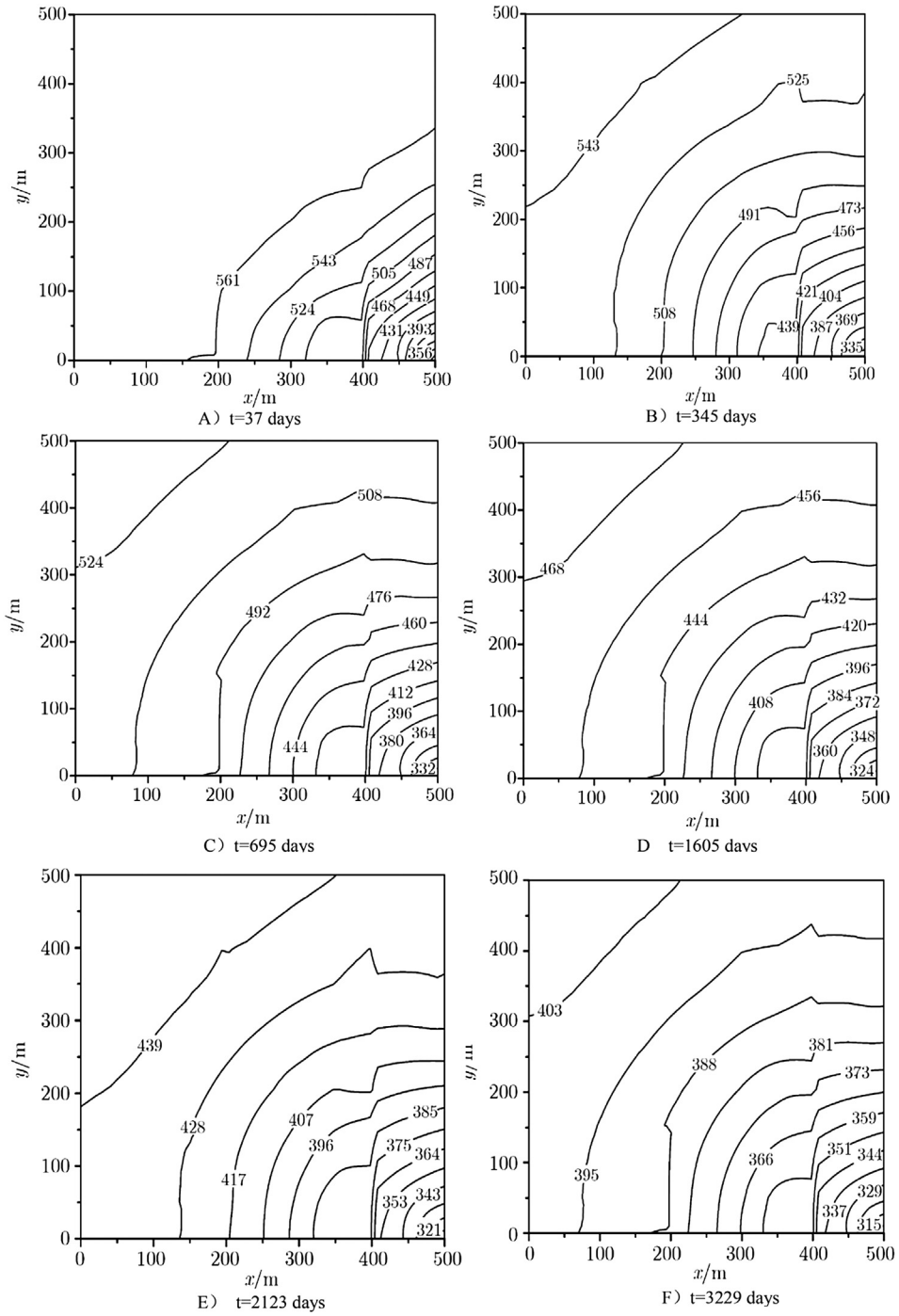


**Fig. 10.** Temperature distribution on the surface of the crack (unit: K). Coordinate of wells: production well (x = 500, y = 500), injection well (x = 0, y = 0).

logarithmically with time as shown in Fig. 18. The fracture aperture increased rapidly during the first year of operation, reaching 110 μm, with a growth rate of over 100%. In subsequent years the growth rate gradually decreased and the width of the fracture became constant after 3 years, at about 150 μm. Thus, the permeability coefficient increased by a factor of nine according to a square law of the fracture. Consequently, the fracture aperture increased with geothermal extraction, the fracture penetration resistance decreased, and the permeability coefficient increased. This further reduced the pressure of the injected water and reduced the energy consumption, increasing the efficiency of the geothermal energy source extraction. This result agrees with the results of Ghassemi [11] although here the fracture aperture changes by a factor of 3 while in Ghassemi the aperture changes only by 1.6 times. It can be assumed that the stratum depth is larger and the temperature is higher in this study. In the process of geothermal energy extraction, the drop of temperature is larger; therefore, the difference in the fracture aperture is larger. Additionally, the evolution of the fracture aperture with time is different; Ghassemi [11] showed that the fracture aperture significantly increased after the geothermal

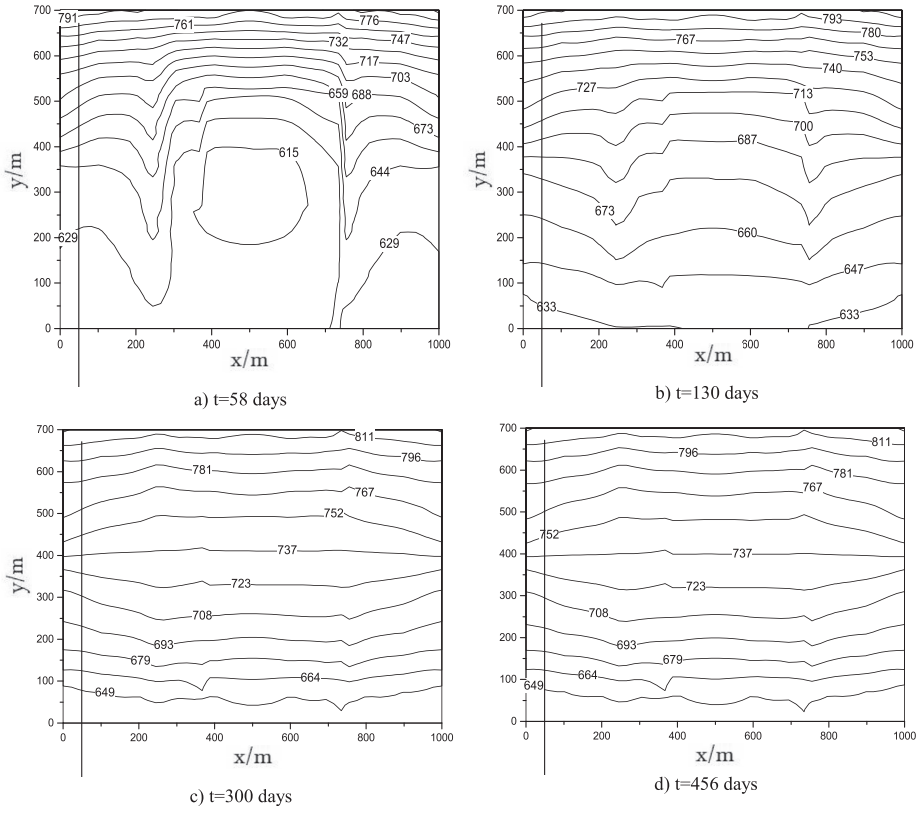


**Fig. 11.** Water pressure distribution on the section between injection well (y = 700) and production well (y = 0) (unit: MPa/10).

extraction, while in our study the fracture aperture tended to stabilize. This may be related to the simplification of the calculation model.

### 4.7. Output and lifespan of the geothermal field

The injection well, production well, artificial storage layer, and the geothermal power plant (or other geothermal utilization facility) constitute a complete HDR geothermal extraction system. An artificial storage layer can be created by drilling in the deep HDR crustal mass and creating giant artificial fracturing. The output is defined as the amount of geothermal energy extracted per unit time throughout the operation period of the system. More specifically, the output is the installed capacity of the terrestrial power plant that can be used by the geothermal extraction system. The lifespan is the period of service of the power plant until the potential geothermal resource is depleted.

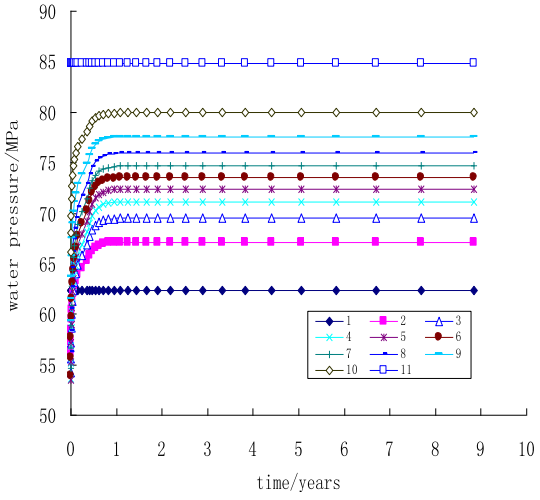


**Fig. 12.** Water pressure different locations on fracture over time Figures notes is number of point on fracture at Fig. 6.

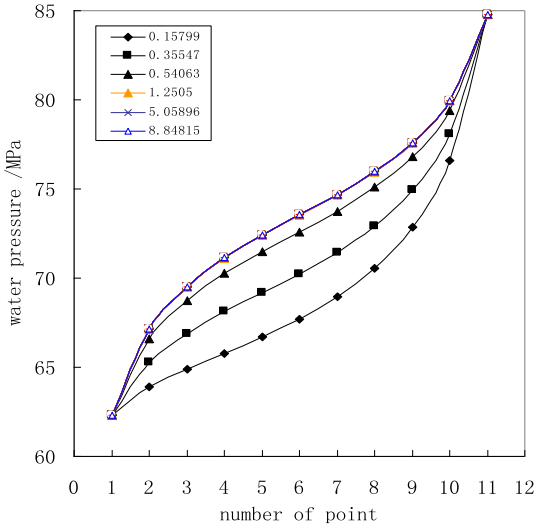


**Fig. 13.** Water pressure at different time (unit: year) at different point on fracture at Fig. 6.

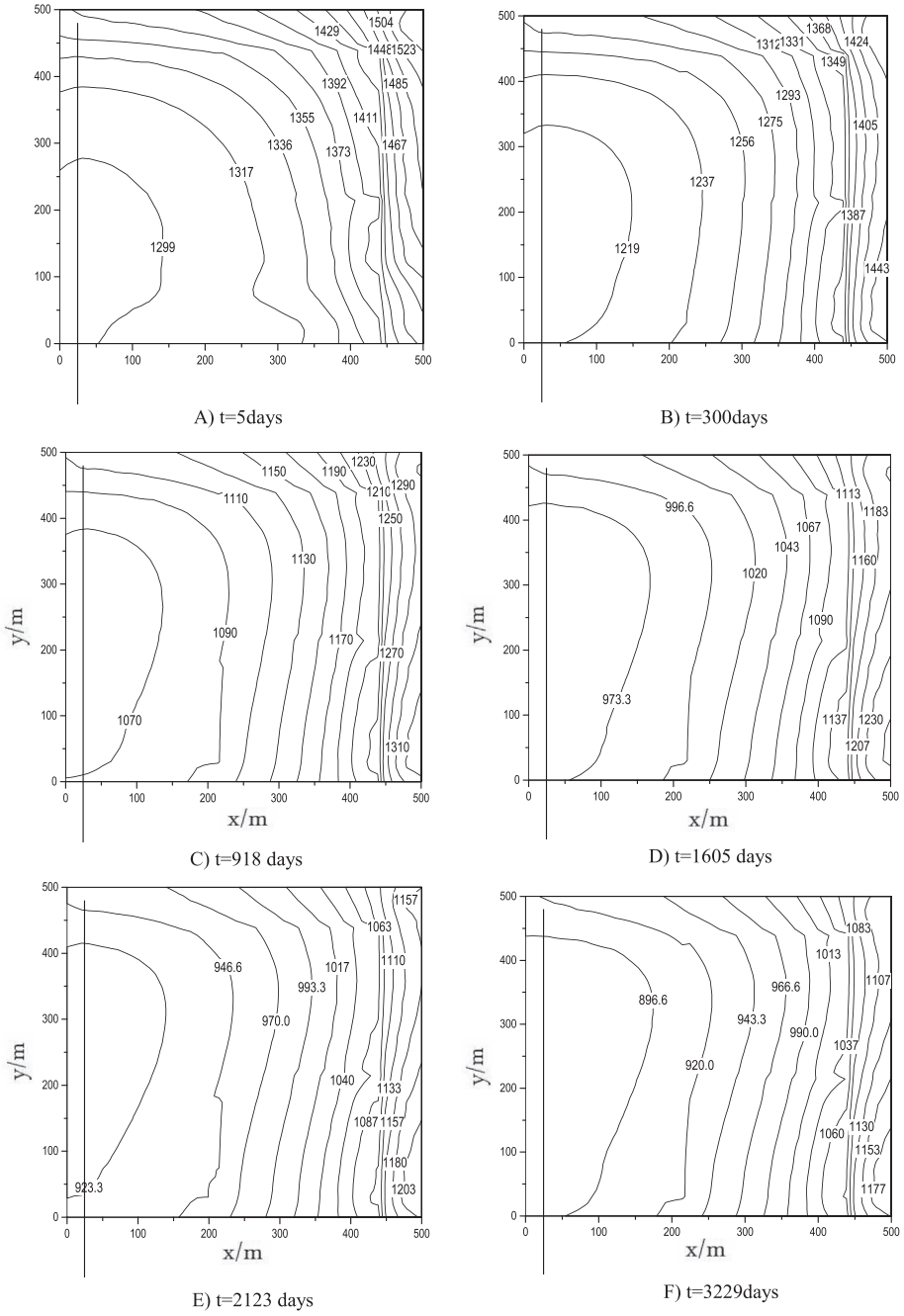


**Fig. 14.** Normal stress distribution on the surface of the crack (unit: MPa/10). Coordinate of wells: production well (x = 500, y = 500), injection well (x = 0, y = 0).

There are two main factors impacting the output and lifespan of an HDR geothermal extraction system: 1) objective factors such as the heat capacity coefficient of the crustal rock mass, original temperature, the temperature gradient, and the spatial distribution range of the HDR. 2) Subjective factors such as drilling depth and the spatial scale of the artificial storage layer. The former is determined mainly by engineering factors such as geophysical parameters, tectonics, site selection, and exploration; the latter involves mainly engineering factors such as deep drilling of the directional well, crustal stress measuring, and giant hydraulic fracturing. Deep drilling can use a rock mass area of higher temperature; giant hydraulic fracturing can create an enormous heat exchange area, ensuring rapid warming of the injected water and a large heat transfer area of the artificial storage layer that will maintain the high temperature for long-term operation of the heat extraction system.

To evaluate the output and lifespan of the HDR geothermal extraction system, we created a numerical model that simulated the process of heat exchange, whereby low-temperature water injected into the artificial storage layer through the injection well was heated, generating superheated water, then discharged from the production well, and finally reached the water heat exchange generator. By analyzing different hot water extraction plans, we examined the temperature variation and distribution in the

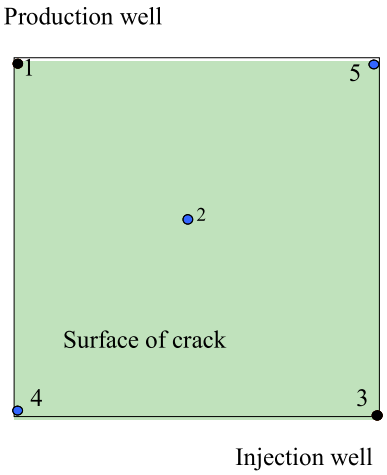


**Fig. 15.** Sketch map of 1–5# representative unit, which is perpendicular to the section of injection well and production well.

artificial storage layer and wall rock, and the lifespan of the artificial storage layer heat extraction system. The output and lifespan parameters were determined by multiple numerical experiments, and the results can be used in the design of hot dry rock geothermal

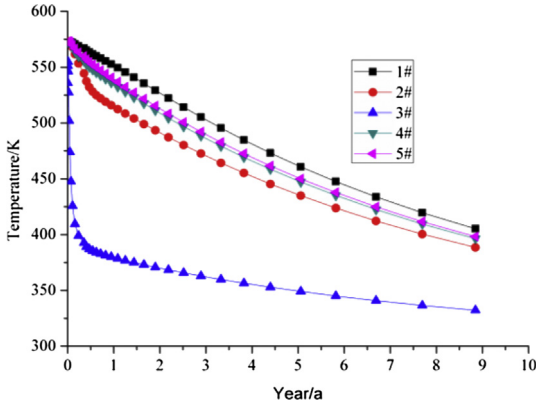


**Fig. 16.** Temperature distributions on the surface of crack with extraction time.

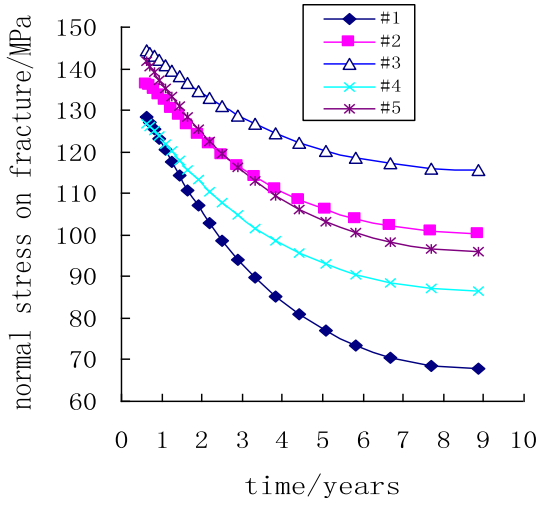


**Fig. 17.** The normal stress on fracture over time. Figure note is point number at Fig. 15.

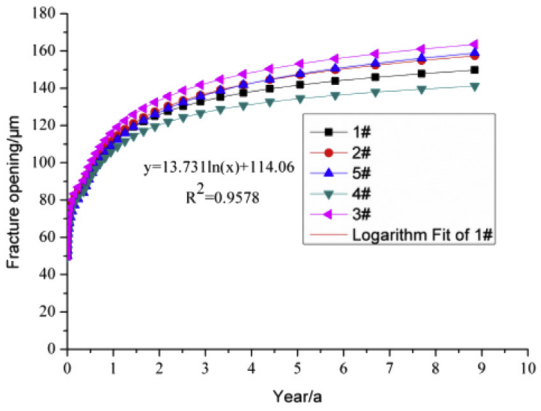


**Fig. 18.** Fracture opening of points over time. Figure note is point number at Fig. 15.

extraction systems. To obtain reliable output and lifespan parameters, we performed cyclic running of the geothermal extraction model that included a large artificial storage layer.

The correlation between the output and lifespan of the HDR geothermal extraction system can be expressed as follows:

$$t_a = f(T_0, dT/dh, V_0, E_t) \tag{10}$$

where $t_a$ is the lifespan; $T_0$ is the original temperature of the artificial storage layer; $dT/dh$ is the geothermal gradient; $V_0$ is the volume of the artificial storage layer; and $E_t$ is the system output, namely the HDR geothermal extraction system's extracted energy

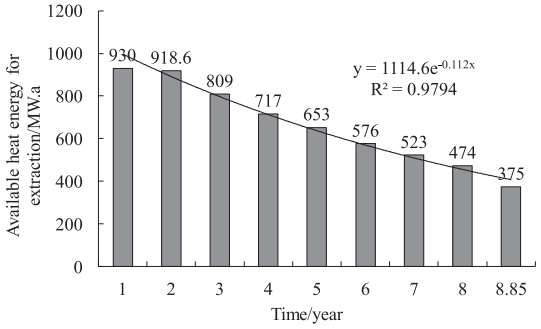


**Fig. 19.** Thermal energy extraction amount by mining system each year.

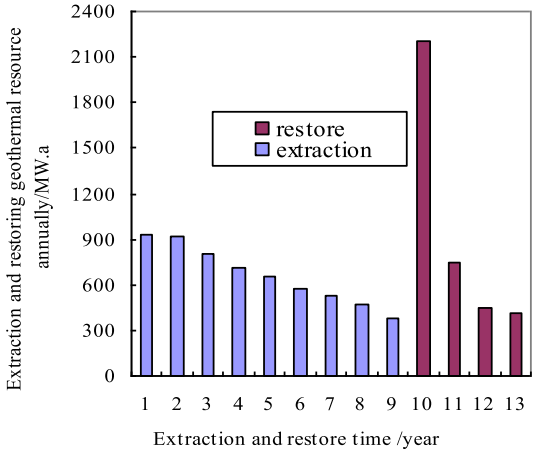


**Fig. 20.** Heat extraction and recovery over time.

per unit time throughout its operational period in Mw/a. We used the numerical model described above to simulate the HDR rock geothermal extraction. The results are shown in Fig. 19. The amount of geothermal energy extracted declined exponentially with time; the fitting function formula can be expressed as $Q = 1114.6e^{-0.1112t}$. The total geothermal resources extracted were 5977 MWa over 9 years. Hence, a geothermal power plant of $50 \times 10^4$ kW will have an expected lifespan of 10 years of service.

The decline rate of the extracted geothermal energy depends mainly on the volume of the artificial storage layer and can be obtained by analyzing the temperature variation of the artificial storage layer. For a small-volume artificial storage layer, the rock mass heat conduction supply rate surrounding the artificial storage layer was not sufficient to meet the geothermal extraction rate because of higher output, causing the output of the HDR geothermal extraction system to rapidly decrease. However, the heat energy of the artificial storage layer quickly recovered when the system stopped extracting geothermal resources for some time. Thus, the system may also maintain geothermal extraction for a longer period. For a simplified HDR geothermal extraction system, the efficiency of extracting heat in this system was very low after running for 9 years. Therefore, we investigated the geothermal reservoir recovery process for an artificial storage layer and wall rock of the HDR geothermal extraction system after stopping the geothermal extraction in the numerical simulation. The calculated results are shown in Fig. 20. The numerical simulation shows that over 4 years, the geothermal reservoir recovered geothermal energy of 3815.5 MWa. This account for 63.8% of the total energy extracted over 9 years and is 13% higher than that of the previous 4 years. In particular, in the first year of recovery, the geothermal energy recovered was very high, reaching 2205 MWa, which accounts for 37% of heat energy extracted over the whole 9 years, and 58% of that recovered in the first 4 years.

The above analyses demonstrate that energy recovery from the artificial storage layer after the extraction stopped was rapid. Consequently, the design of HDR geothermal extraction systems should consider alternating between system heat extraction and recovery. Therefore, an HDR geothermal power plant should establish at least two sets of geothermal extraction systems for heat; with extraction and recovery of two sets of systems running alternately, the output and lifespan of the HDR geothermal extraction system can be greatly improved ensuring continuous energy supply.

## 5. Conclusions

Based on the geothermal energy extraction plan of the Chinese Tengchong geothermal field, we investigated the variation of the temperature field, stress field, seepage field, and fracture aperture during HDR geothermal extraction through numerical simulations. The numerical model was based on THM coupling of HDR geothermal extraction. The main findings are summarized as follows:

(1) Geothermal extraction was performed at the Tengchong geothermal field with a geothermal gradient of 50 K/km, at depths of 6250–6750 m and a horizontal length of 1000 m by simulating two large vertical cracks to connect the injection and production wells in the Tengchong geothermal field. The temperature along the fracture face increased from the injection well towards the production well in the process of geothermal extraction. The temperature increase was exponential with the distance between the injection well and the production well. The temperature of a large area near the injection well decreased linearly with time. The initial temperature of the rock mass was 575 K, and temperature decreased to 423 K after 9 years of geothermal extraction.

(2) The initial water pressure gradient in the fracture reached 0.17 MPa/m near the injection well. After 1 year of geothermal extraction the pressure gradient decreased to 0.052 MPa/m, and the fracture aperture was three times the initial aperture. The results indicate that the seepage resistance of the artificial storage layer gradually decreased with the continuation of geothermal extraction; hence the geothermal energy extraction process became more efficient.

(3) The amount of extracted geothermal energy declined exponentially with time, as $Q = 1114.6 \exp(-0.1112t)$. The total geothermal energy extracted over the 9-year period was 5977 MWa while the rock mass temperature decreased from initial 573 K–423 K. The geothermal energy recovered from the artificial storage layer in the 4-year period after the extraction stopped accounted for 64% of the total energy extracted over the 9-year extraction period. In particular, the recovery during the first year accounted for 37% of the total extracted heat over 9 years. These results suggest that in HRD geothermal extraction, two artificial storage layers should be established simultaneously for alternate extraction, thus obtaining very high efficiency of geothermal resource extraction.

As a kind of new energy, there is no practical engineering for extracting hot dry rock geothermal energy to be implemented, whose pressure and temperature conditions are mentioned in the paper. Hence, it is hard to find the practical data to validate the results. However, the authors insist on that the more potential and valuable hot dry rock geothermal energy is that whose temperature is greater than 573 K and correspondent depth is 6000 m–7000 m. In order to develop it, the mainly only way is to develop the theory first. So it is helpful for extracting deeper and higher temperature geothermal energy to discover new phenomena via conducting numerical simulation on the strength of scientific theory.

## Acknowledgments

This study was supported by the project of China National Science Foundation (Grant No. 5122540 and 51404161).

## References

[1] Duchane D. Hot dry rock: a realistic energy option. Geotherm Counc Bull 1990;19(3):83–8.
[2] Duchane D. International programs in hot dry rock technology development. Geotherm Counc Bull 1991;20(5):135–42.
[3] Brown DW. Recent testing of the HDR reservoir at Fenton Hill New Mexico. Geotherm Counc Bull 1993;22(9):208–14.
[4] Kohl T, Evans KF, Hopkirk RJ, Rybach L. Coupled hydraulic, thermal and mechanical consideration for the simulation of hot dry rock reservoirs. Geothermics 1995;24(3):343–59.
[5] Zeng YC, Su Z, Wu NY. Numerical simulation of heat production potential from hot dry rock by water circulating through two horizontal wells at desert peak geothermal field. Energy 2013;56:92–107.
[6] Zeng YC, Wu NY, Zheng Su, Wang XX, Hu J. Numerical simulation of heat production potential from hot dry rock by water circulating through a novel single vertical fracture at desert peak geothermal field. Energy 2013;63:268–82.
[7] Chamorro CR, Mondejar ME, Ramos R, Segovia JJ, Martin MC, Villamanan MA. World geothermal power status: energy, environmental and economic study of high enthalpy technologies. Energy 2012;42(1):10–8.
[8] Fox DB, Sutter D, Beckers KF, Lukawski MZ, Koch DL, Anderson BJ, Tester JW. Sustainable heat farming: modeling extraction and recovery in discretely fractured geothermal reservoirs. Geothermics 2013;46:42–54.
[9] Chamorro CR, Garcia-Cuesta JL, Mondejar ME, Linares MM. An estimation of the enhanced geothermal systems potential for the Iberian Peninsula. Renew Energy 2014;66:1–14.

[10] Pandey SN, Chaudhuri A, Kelkar S, Sandeep VR, Rajaram H. Investigation of permeability alteration of fractured limestone reservoir due to geothermal heat extraction using three-dimensional thermo-hydro-chemical (T -HC) model. Geothermics 2014;51:46–62.
[11] Ghassemi A, Zhou X. A three dimensional thermo-poroelastic model for fracture response to injection/extraction in enhanced geothermal system. Geothermics 2011;40:39–49.
[12] Zhao YS, Wan ZJ, Kang JR. Introduction to HDR geothermal development. Beijing: Science Press; 2004.
[13] Wan ZJ, Zhao YS, Kang JR. Forecast and evaluation of hot dry rock geothermal resource in China. Renew Energy 2005;30:1831–46.
[14] Feng ZJ, Zhao YS, Zhou AC, Zhang N. Development program of hot dry rock geothermal resource in the Yangbajing basin of China. Renew Energy 2012;39:490–5.
[15] Taron J, Elsworth D, Min KB. Numerical simulation of thermal- hydrologic –mechanical -chemical processes in deformable, fractured porous media. Int J Rock Mech Min Sci 2009;46:842–54.